18th International Specialty Conference on Cold-Formed Steel Structures
October 26-27, 2006, Orlando, Florida

Buckling analysis of cold-formed steel members using CUFSM: conventional and constrained finite strip methods

B.W. Schafer[1] and S. Ádány[2]

Abstract

The objective of this paper is to provide technical background and illustrative examples for stability analysis of cold-formed steel members using the conventional and constrained finite strip methods as implemented in the open source program CUFSM. Numerical stability analysis combined with an accurate identification of the buckling modes is an enabling first step in the implementation of new design methods such as the Direct Strength Method. In this paper conventional finite strip method analysis identical to that employed in CUFSM is derived from first principles. The methodology closely mirrors that of standard matrix methods for structural analysis, widely used by engineers, and can be readily programmed by the interested reader. An example of the stability solution for an industry standard lipped channel is provided. Recently, CUFSM has been extended to include application of the constrained finite strip method. Using formal mechanical definitions of the buckling classes: global, distortional, local, and other deformations, the constrained finite strip method can provide both modal decomposition and modal identification to a conventional finite strip solution. Modal decomposition allows the conventional finite strip solution to be focused on any buckling class (e.g., global, distortional, or local only), resulting in problems of reduced size and definitive solutions for the buckling modes in isolation, as demonstrated for an example section. Modal identification allows the results of a conventional finite strip solution to be judged with regard to the participation of the buckling classes; and thus provide a measure of buckling mode interaction. The conventional finite strip method combined with the constrained finite strip method provides a powerful tool for understanding cross-section stability in cold-formed steel members.

[1] Associate Professor, Johns Hopkins University, United States, schafer@jhu.edu
[2] Associate Professor, Budapest University of Technology and Economics, Hungary, sadany@epito.bme.hu

Introduction

Cold-formed steel members are thin, light, and efficient. However, this efficiency comes with complication: engineers must consider buckling of the thin walls of the cross-section in addition to global (e.g., flexural or lateral-torsional) buckling of the member. Classical hand solutions to these instabilities become unduly cumbersome for more complex buckling modes, such as distortional buckling; and may ignore critical mechanical features, such as inter-element equilibrium and compatibility. To remedy this, the engineer may turn to numerical solutions such as the finite strip method (FSM).

Conventional FSM provides a means to examine all the possible instabilities in a cold-formed steel member under longitudinal stresses (axial, bending, or combinations thereof). CUFSM is an open source FSM program, freely available from the first author of this paper, that provides engineers with this capability (www.ce.jhu.edu/bschafer/cufsm). The basic framework of the FSM stability solution will be familiar to anyone who has studied matrix structural analysis. In this paper the underlying elastic and geometric stiffness matrices are derived and shown in closed-form so that users can become more familiar with this tool and more comfortable with employing FSM solutions in design. In addition, an example of a conventional FSM solution is provided. New design methods such as the Direct Strength Method become highly efficient for the engineer when FSM stability solutions are employed.

Recently, extensions to the conventional FSM solution have been explored, namely, the constrained finite strip method, or *c*FSM. A *c*FSM solution provides a means for (1) stability solutions to be focused only a given buckling mode (*modal decomposition*), or (2) a conventional FSM stability solution may be classified into the different fundamental buckling modes (*modal identification*). Modal decomposition is accomplished by forming a series of constraint equations which describe a particular buckling class, i.e., local, distortional, or global buckling. A conventional FSM solution is then constrained to the selected buckling class and stability analysis performed. Since the number of degrees of freedom (DOF) within a class are much less than the full model, modal decomposition also results in significant model reduction. In this paper the criteria used to define the classes are provided, and implementation of the constraints is demonstrated. Modal identification employs the developed constraint equations as a means to transform the solution basis from the nodal DOF to modal DOF associated with the classes. This allows a buckling mode to be identified in terms of its contribution from the different classes. Formal definition and an example of modal identification are provided. The implementation of *c*FSM discussed herein is completed in CUFSM.

Conventional Finite Strip Method

In the finite strip method (FSM) a thin-walled member, such as the lipped channel of Figure 1, is discretized into longitudinal strips. The advantage of FSM over other methods, such as the finite element method which applies discretization in both the longitudinal and transverse direction, is dependent on a judicious choice of the shape function for the longitudinal displacement field. In Figure 1 a single strip is highlighted, along with the degrees of freedom (DOF) for the strip, the dimensions of the strip, and applied edge tractions (loads).

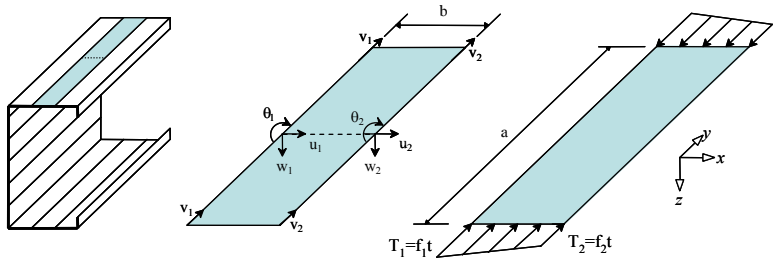

Figure 1 Finite strip discretization, strip DOF, dimensions, and applied edge tractions

Elastic stiffness matrices

The vector of general displacement fields: $\mathbf{u} = [u\ v\ w]^T$ is approximated by the displacement at the nodes, **d**, and selected shape functions, **N**, via

$$\mathbf{u} = \mathbf{N}\mathbf{d} = [\mathbf{N_{uv}}\ \mathbf{N_w}]\ [\mathbf{d_{uv}}^T \mid \mathbf{d_{w\theta}}^T]^T$$

where the nodal displacements in local coordinates are shown in Figure 1 and may be explicitly written as $\mathbf{d} = [u_1\ v_1\ u_2\ v_2 \mid w_1\ \theta_1\ w_2\ \theta_2]^T$ or in partitioned form $\mathbf{d} = [\mathbf{d_{uv}}^T \mid \mathbf{d_{w\theta}}^T]^T$. For the in-plane, or membrane, displacements *u* and *v* linear shape functions are employed in the transverse direction, and in the longitudinal direction *u* employs a sin function and *v* a cos function for displacement:

$$u = \left[\left(1-\frac{x}{b}\right)\ \ \left(\frac{x}{b}\right)\right]\begin{Bmatrix}u_1\\u_2\end{Bmatrix}\sin\left(\frac{m\pi y}{a}\right),\ v = \left[\left(1-\frac{x}{b}\right)\ \ \left(\frac{x}{b}\right)\right]\begin{Bmatrix}v_1\\v_2\end{Bmatrix}\cos\left(\frac{m\pi y}{a}\right)$$

Out-of-plane displacement, *w*, is approximated by a cubic polynomial:

$$w = \left[\left(1-\frac{3x^2}{b^2}+\frac{2x^3}{b^3}\right)\ \ x\left(1-\frac{2x}{b}+\frac{x^2}{b^2}\right)\ \ \left(\frac{3x^2}{b^2}-\frac{2x^3}{b^3}\right)\ \ x\left(\frac{x^2}{b^2}-\frac{x}{b}\right)\right]\begin{Bmatrix}w_1\\\theta_1\\w_2\\\theta_2\end{Bmatrix}sin\left(\frac{m\pi y}{a}\right)$$

The strain in the strip is decomposed into two portions: membrane and bending. The membrane strains, $\boldsymbol{\varepsilon_m}$, are at the mid-line of the strip and are governed by plane stress assumptions. The bending strains, $\boldsymbol{\varepsilon_b}$, follow Kirchoff thin plate theory and are zero at the mid-line and a function of *w* alone.

$$\boldsymbol{\varepsilon} = \boldsymbol{\varepsilon_m} + \boldsymbol{\varepsilon_b}$$

$$\boldsymbol{\varepsilon_m} = \begin{Bmatrix} \varepsilon_x \\ \varepsilon_y \\ \gamma_{xy} \end{Bmatrix}_m = \begin{Bmatrix} \partial u/\partial x \\ \partial v/\partial y \\ \partial u/\partial y + \partial v/\partial x \end{Bmatrix} = \mathbf{N}'_{\mathbf{uv}}\mathbf{d}_{\mathbf{uv}} = \mathbf{B}_{\mathbf{m}}\mathbf{d}_{\mathbf{uv}}$$

$$\boldsymbol{\varepsilon_b} = \begin{Bmatrix} \varepsilon_x \\ \varepsilon_y \\ \gamma_{xy} \end{Bmatrix}_b = \begin{Bmatrix} -z\partial^2 w/\partial x^2 \\ -z\partial^2 w/\partial y^2 \\ 2z\partial^2 w/\partial x\partial y \end{Bmatrix} = \mathbf{N}''_{\mathbf{w}}\mathbf{d}_{\mathbf{w\theta}} = \mathbf{B}_{\mathbf{b}}\mathbf{d}_{\mathbf{w\theta}}$$

As shown above $\boldsymbol{\varepsilon_m}$ and $\boldsymbol{\varepsilon_b}$ may be written in terms of appropriate derivatives of the shape functions, **N**, and the nodal displacements, **d**. The elastic stiffness may be understood through a statement of internal strain energy:

$$U = \tfrac{1}{2}\int \boldsymbol{\sigma}^{\mathbf{T}}\boldsymbol{\varepsilon} dV = \tfrac{1}{2}\int \boldsymbol{\varepsilon}^{\mathbf{T}}\mathbf{E}\boldsymbol{\varepsilon} dV = \tfrac{1}{2}\mathbf{d}^{\mathbf{T}}\int \mathbf{B}^{\mathbf{T}}\mathbf{E}\mathbf{B} dV \mathbf{d} = \tfrac{1}{2}\mathbf{d}^{\mathbf{T}}\mathbf{k}_{\mathbf{e}}\mathbf{d}$$

Where the stress is connected to the strain by an orthotropic plane stress constitutive relation: $\boldsymbol{\sigma} = \mathbf{E}\boldsymbol{\varepsilon}$, and $\mathbf{E}=\mathbf{E}^{\mathrm{T}}$. Since the membrane behavior (*u*, *v*) is uncoupled from the bending behavior (*w*) separate elastic stiffness matrices may be derived for each, where

$$\mathbf{k}_{\mathbf{e}} = \begin{bmatrix} \mathbf{k}_{\mathbf{em}} & \mathbf{0} \\ \mathbf{0} & \mathbf{k}_{\mathbf{eb}} \end{bmatrix}$$

$$\mathbf{k}_{\mathbf{em}} = \int \mathbf{B}_{\mathbf{m}}^{\mathrm{T}}\mathbf{E}\mathbf{B}_{\mathbf{m}} dV \quad \text{and} \quad \mathbf{k}_{\mathbf{eb}} = \int \mathbf{B}_{\mathbf{b}}^{\mathrm{T}}\mathbf{E}\mathbf{B}_{\mathbf{b}} dV$$

Substitution and integration leads to the following closed-formed solution for the membrane, $\mathbf{k}_{\mathbf{em}}$, and bending, $\mathbf{k}_{\mathbf{eb}}$, elastic stiffness matrices:

$$\mathbf{k}_{\mathbf{em}} = t\begin{bmatrix} \left(\frac{aE_1}{2b} + \frac{abk_m^2 G}{6}\right) & & & \text{symmetric} \\ \left(\frac{ak_m \nu_x E_2}{4} - \frac{ak_m G}{4}\right) & \left(\frac{abk_m^2 E_2}{6} + \frac{aG}{2b}\right) & & \\ \left(-\frac{aE_1}{2b} + \frac{abk^2 G}{12}\right) & \left(-\frac{ak_m \nu_x E_2}{4} - \frac{ak_m G}{4}\right) & \left(\frac{aE_1}{2b} + \frac{abk_m^2 G}{6}\right) & \\ \left(\frac{ak_m \nu_x E_2}{4} + \frac{ak_m G}{4}\right) & \left(\frac{abk_m^2 E_2}{12} - \frac{aG}{2b}\right) & \left(-\frac{ak_m \nu_x E_2}{4} + \frac{ak_m G}{4}\right) & \left(\frac{abk_m^2 E_2}{6} + \frac{aG}{2b}\right) \end{bmatrix}$$

where: $k_m = \frac{m\pi}{a} \quad E_1 = \frac{E_x}{1-\nu_x\nu_y} \quad E_2 = \frac{E_y}{1-\nu_x\nu_y}$

$$\mathbf{k}_{\mathbf{eb}} = \begin{bmatrix} \left(\frac{13ab}{70}k_m^4 D_y + \frac{12a}{5b}k_m^2 D_{xy} + \frac{6a}{5b}k_m^2 D_1 + \frac{6a}{b^3}D_x\right) & & & \text{symmetric} \\ \left(\frac{3a}{5}k_m^2 D_1 + \frac{a}{5}k_m^2 D_{xy} + \frac{3a}{b^2}D_x + \frac{11ab^2}{420}k_m^4 D_y\right) & \left(\frac{ab^3}{210}k_m^4 D_y + \frac{4ab}{15}k_m^2 D_{xy} + \frac{2ab}{15}k_m^2 D_1 + \frac{2a}{b}D_x\right) & & \\ \left(\frac{9ab}{140}k_m^4 D_y - \frac{12a}{5b}k_m^2 D_{xy} - \frac{6a}{5b}k_m^2 D_1 - \frac{6a}{b^3}D_x\right) & \left(\frac{13ab^2}{840}k_m^4 D_y - \frac{a}{5}k_m^2 D_{xy} - \frac{a}{10}k_m^2 D_1 - \frac{3a}{b^2}D_x\right) & \left(\frac{13ab}{70}k_m^4 D_y + \frac{12a}{5b}k_m^2 D_{xy} + \frac{6a}{5b}k_m^2 D_1 + \frac{6a}{b^3}D_x\right) & \\ \left(-\frac{13ab^2}{840}k_m^4 D_y + \frac{a}{5}k_m^2 D_{xy} + \frac{a}{10}k_m^2 D_1 + \frac{3a}{b^2}D_x\right) & \left(-\frac{3ab^3}{840}k_m^4 D_y - \frac{ab}{15}k_m^2 D_{xy} - \frac{ab}{30}k_m^2 D_1 + \frac{a}{b}D_x\right) & \left(-\frac{11ab^2}{420}k_m^4 D_y - \frac{a}{5}k_m^2 D_{xy} - \frac{3a}{5}k_m^2 D_1 - \frac{3a}{b^2}D_x\right) & \left(\frac{ab^3}{210}k_m^4 D_y + \frac{4ab}{15}k_m^2 D_{xy} + \frac{2ab}{15}k_m^2 D_1 + \frac{2a}{b}D_x\right) \end{bmatrix}$$

where: $k_m = \frac{m\pi}{a}$ $D_x = \frac{E_x t^3}{12(1-\nu_x\nu_y)}$ $D_y = \frac{E_y t^3}{12(1-\nu_x\nu_y)}$ $D_{xy} = \frac{Gt^3}{12}$ $D_1 = \frac{\nu_y E_x t^3}{12(1-\nu_x\nu_y)} = \frac{\nu_x E_y t^3}{12(1-\nu_x\nu_y)}$

Geometric stiffness matrices

Consider the member to be loaded with linearly varying edge tractions (T_1, T_2) as shown in Figure 1. The geometric stiffness matrix may be determined by considering the additional potential energy incurred as these edge tractions displace longitudinally (in the y direction); or equivalently in terms of higher-order strain definitions (i.e., the Green-Lagrange strain):

$$W = \int_0^a \int_0^b \left(T_1 - (T_1 - T_2)\frac{x}{b}\right)\frac{1}{2}\left(\left(\frac{\partial u}{\partial y}\right)^2 + \left(\frac{\partial v}{\partial y}\right)^2 + \left(\frac{\partial w}{\partial y}\right)^2\right)dxdy$$

The derivatives of the displacement fields may be written in terms of derivatives of the shape functions, **N**, and nodal displacements, **d**, similar to the elastic stiffness solution. For example, for bending, *w*:

$$\left(\frac{\partial w}{\partial y}\right)^2 = \mathbf{d}_{\mathbf{w\theta}}{}^T \mathbf{N}_{\mathbf{w}}'{}^T \mathbf{N}_{\mathbf{w}}' \mathbf{d}_{\mathbf{w\theta}} = \mathbf{d}_{\mathbf{w\theta}}{}^T \mathbf{G}_{\mathbf{b}}{}^T \mathbf{G}_{\mathbf{b}} \mathbf{d}_{\mathbf{w\theta}}$$

Introducing this notation into the earlier potential energy statement leads to a formal definition of the geometric stiffness matrix, $\mathbf{k_g}$.

$$W = \frac{1}{2}\mathbf{d}^T \int_0^a \int_0^b \left(T_1 - (T_1 - T_2)\frac{x}{b}\right)\mathbf{G}^T\mathbf{G}dxdy\mathbf{d} = \frac{1}{2}\mathbf{d}^T\mathbf{k}_{\mathbf{g}}\mathbf{d}$$

Similar to the elastic stiffness matrix, $\mathbf{k_g}$ may be broken into two parts. One related to the *u* and *v* displacement fields, or membrane deformations, $\mathbf{k_{gm}}$, and one related to *w*, or bending, $\mathbf{k_{gb}}$:

$$\mathbf{k_{gm}} = \int_0^a \int_0^b \left(T_1 - (T_1 - T_2)\frac{x}{b} \right) \mathbf{G_m}^T \mathbf{G_m} dxdy$$

$$\mathbf{k_{gb}} = \int_0^a \int_0^b \left(T_1 - (T_1 - T_2)\frac{x}{b} \right) \mathbf{G_b}^T \mathbf{G_b} dxdy$$

Substitution and subsequent integration lead to the following closed-form expressions for the geometric stiffness matrices:

$$\mathbf{k_{gm}} = C \begin{bmatrix} 70(3T_1 + T_2) & 0 & 70(T_1 + T_2) & 0 \\ & 70(3T_1 + T_2) & 0 & 70(T_1 + T_2) \\ & & 70(T_1 + 3T_2) & 0 \\ \text{symmetric} & & & 70(T_1 + 3T_2) \end{bmatrix}$$

$$\mathbf{k_{gb}} = C \begin{bmatrix} 8(30T_1 + 9T_2) & 2b(15T_1 + 7T_2) & 54(T_1 + T_2) & -2b(7T_1 + 6T_2) \\ & b^2(5T_1 + 3T_2) & 2b(6T_1 + 7T_2) & -3b^2(T_1 + T_2) \\ & & 24(3T_1 + 10T_2) & -2b(7T_1 + 15T_2) \\ \text{symmetric} & & & b^2(3T_1 + 5T_2) \end{bmatrix}$$

where: $C = b(m\pi)^2 / 1680a$

Global stiffness matrices and assembly

To form the global elastic ($\mathbf{K_e}$) and geometric stiffness ($\mathbf{K_g}$) matrices each individual strip must be transformed from local to global coordinates and then assembled. A note on notation, local DOF are denoted by lowercase u, v, w, θ and global DOF by uppercase U, V, W, Θ; further, stiffness matrices in the strip local coordinate system are a lowercase **k,** and in the global system an uppercase **K** is used. The local to global transformation at node "i" for strip "j" which is oriented in the left-handed coordinate system of Figure 1 at an angle $\alpha^{(j)}$ is governed by the following transformations:

$$\begin{bmatrix} u_i \\ w_i \end{bmatrix} = \begin{bmatrix} \cos\alpha^{(j)} & \sin\alpha^{(j)} \\ -\sin\alpha^{(j)} & \cos\alpha^{(j)} \end{bmatrix} \begin{bmatrix} U_i \\ W_i \end{bmatrix} \text{ and } \begin{bmatrix} v_i \\ \theta_i \end{bmatrix} = \begin{bmatrix} 1 & 0 \\ 0 & 1 \end{bmatrix} \begin{bmatrix} V_i \\ \Theta_i \end{bmatrix}$$

These may be collected into a matrix form for all DOF in strip j as

$$\mathbf{d}^{(j)} = \mathbf{\Gamma}^{(j)} \mathbf{D}^{(j)}$$

Transformation of the stiffness matrices of strip j follows from:

$$\mathbf{K_e}^{(j)} = \mathbf{\Gamma}^{(j)T} \mathbf{k_e}^{(j)} \mathbf{\Gamma}^{(j)} \text{ and } \mathbf{K_g}^{(j)} = \mathbf{\Gamma}^{(j)T} \mathbf{k_g}^{(j)} \mathbf{\Gamma}^{(j)}$$

With all DOF in global coordinates the global stiffness matrices may be assembled as an appropriate summation of the strip stiffness matrices, where:

$$\mathbf{K}_e = \sum_{\text{assembly}}^{j=1 \text{ to } n} \mathbf{K}_e^{(j)} \quad \text{and} \quad \mathbf{K}_g = \sum_{\text{assembly}}^{j=1 \text{ to } n} \mathbf{K}_g^{(j)}$$

Stability solution

For a given distribution of edge tractions on a member the geometric stiffness scales linearly, this leads to the stability eigenvalue problem of interest, which for a single eigen (buckling) mode, $\boldsymbol{\phi}$, and eigen (buckling) value λ may be expressed as:

$$\mathbf{K}_e\boldsymbol{\phi} = \lambda\mathbf{K}_g\boldsymbol{\phi}$$

Both $\mathbf{K}_e$ and $\mathbf{K}_g$ are a function of the strip length, *a*. Therefore, the elastic buckling value and the corresponding buckling modes are also a function of *a*. The problem can be solved for several lengths, *a*, and thus a complete picture of the elastic buckling value and modes can be determined. The minima of such a curve can generally be considered as the critical buckling loads and modes for a member. CUFSM follows this implementation and an example is provided in Figure 2. Given the selected longitudinal shape functions, *a* is generally known as the half-wavelength.

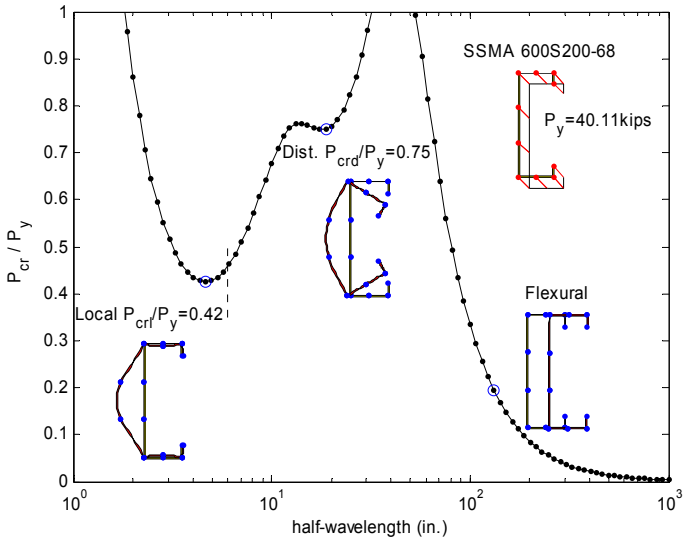

Figure 2 Conventional FSM analysis of an SSMA 600S200-68 structural stud

In the conventional FSM described above the selected shape functions result in members that are pinned and free-to-warp at their ends. More complicated boundary conditions are possible, but require the longitudinal deformations of u, v, w to be defined in terms of a series (or splines) and result in much larger and more complicated eigenvalue problems (see e.g., Bradford and Azhari 1995). Further, more exact treatments of the deformations may employ higher order polynomials for the transverse displacements (e.g., see Rhodes 2002). For a complete treatment of finite strip derivations, and applications beyond member stability, see Cheung and Tham (1998). Finite strip solutions that use the shape functions presented here are the most common in thin-walled stability and will be termed the semi-analytical or conventional FSM. CUFSM (Schafer 2006) provides a solution in this form as does CFS (CFS 2006) and THIN-WALL (Papangelis and Hancock 1995, 2006).

Definition of the buckling classes

As the FSM analysis of Figure 2 demonstrates, stability of cold-formed steel members can typically be categorized into one of three classes: *global* (G), *distortional* (D), or *local* (L). A convenient means for this classification is the minima of the conventional FSM analysis results. However, while convenient, this definition is by no means general and depends on the details of the cross-section and loading. Sometimes minima may not exist, or extra minima may exist. Qualitative definitions for the classes are also possible, for example the Commentary to the Direct Strength Method (Appendix 1 NAS 2004), but again such classifications are not general. Another characterization with some popularity relies on the relative contribution from membrane versus bending effects. For example, the strain energy, broken into terms derived from the membrane ($\mathbf{k}_{em}$) and from bending ($\mathbf{k}_{eb}$) are given in Figure 3 (as provided in CUFSM). As the plots illustrate, each mode class has a certain characterizing energy distribution over the cross-section: e.g., local modes involve only bending strain energy. Definitive classification using any of the above methods remains elusive.

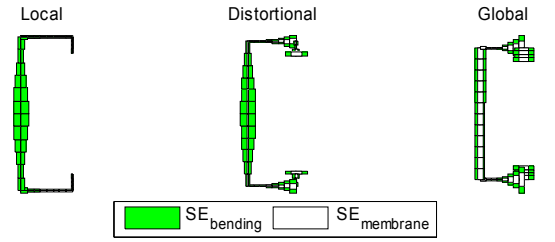

Figure 3 Strain energy related to membrane and bending deformations for the buckling modes

To provide a means of rigorous classification mechanical definitions have been selected. Given the lack of alternative proposals, the criteria applied in generalized beam theory (GBT) are used, (Silvestre and Camotim 2002a,b), which are found to usually be in good agreement with current engineering classifications. The separation of G, D, L and *other* (O) deformation modes are completed through selective implementation of the following three criteria. **Criterion #1**: (a) $(\gamma_{xy})_m = 0$, i.e. there is no in-plane shear, (b) $(\varepsilon_x)_m = 0$, i.e. there is no in-plane transverse strain, and (c) v is linear in x within a flat part (i.e. between any two fold locations). **Criterion #2**: (a) $v \neq 0$, i.e. the warping displacement is not constantly equal to zero along the whole cross-section, and (b) the cross-section is in transverse equilibrium. **Criterion #3**: $\kappa_{xx} = 0$, i.e. there is no transverse flexure.

Table 1 Mode classification criterion

	G modes	**D** modes	**L** modes	**O** modes
Criterion #1 – Vlasov's hypothesis	Yes	Yes	Yes	No
Criterion #2 – Longitudinal warping	Yes	Yes	No	-
Criterion #3 – Undistorted section	Yes	No	-	-

Application of the criterion to the G, D, L, and O buckling mode classes is defined in Table 1. Criterion 1 may be understood as being tied to classical beam theory, or, Vlasov's hypothesis, and restricts certain membrane deformations, while allowing warping. Criterion 2 implies that warping (longitudinal, or v deformation) must be non-zero, thus providing a separation between local plate deformations which have no deformation at the mid-plane of the plate and other deformation modes. Criterion 3 relates to distortion of the cross-section and provides a means to separate G from D. While the modes implied by these criteria are in accordance with current practice for a wide range of practical problems; cases do exist where the applied definition leads to results not in-line with current engineering practice. Further comparison of *c*FSM with GBT is provided in Ádány et al. (2006).

Constrained Finite Strip Method

Application of buckling classes through constraints

Consider the membrane deformations $\mathbf{d_{uv}}$ of a single finite strip, as shown in Figure 4. Introducing the first constraint from criterion #1, $(\varepsilon_x)_m=0$ results in

$$\left(\varepsilon_x\right)_m = \frac{\partial u}{\partial x} = \frac{-u_1 + u_2}{b} \sin\frac{m\pi y}{a} = 0$$

and since the sine function is generally not equal to zero, u_1 and u_2 must be equal to each other in order to satisfy the equality. This implies that the transverse displacements of the strip's two nodal lines must be identical, which is a natural consequence of the zero transverse strain assumption. In practice, the identical u displacements prevent those deformations where the two longitudinal edges of the strip are not parallel, as illustrated in Figure 4.

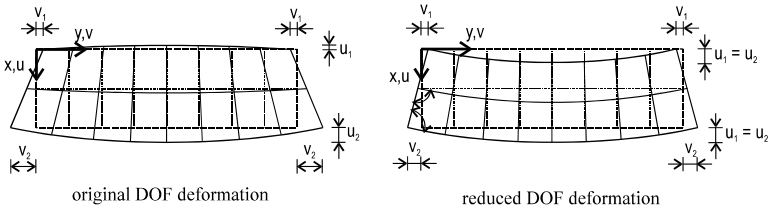

Figure 4. Effect of $(\varepsilon_x)_m = 0$ strain constraint on membrane deformations

The above derivation demonstrates that the introduction of a strain constraint reduces the number of DOF, in this particular case from 4 to 3. Thus, we can define the new, reduced DOF by u, v_1 and v_2, while the relationship of the original and reduced displacement vectors can be expressed as follows:

$$\begin{bmatrix} u_1 \\ v_1 \\ u_2 \\ v_2 \end{bmatrix} = \begin{bmatrix} 1 & 0 & 0 \\ 0 & 1 & 0 \\ 1 & 0 & 0 \\ 0 & 0 & 1 \end{bmatrix} \begin{bmatrix} u \\ v_1 \\ v_2 \end{bmatrix} \quad \text{or} \quad \mathbf{d_{uv}} = \mathbf{R}\mathbf{d_{uv\text{-}r}}$$

where **R** is the constraint matrix, which is a representation of the introduced strain constraints. For more general strain-displacement constraints (i.e., the other criteria), and more general cross-sections, the derivations are more complicated, but finally the associated constraint matrices (**R**) can be defined, as shown in Ádány and Schafer (2006a,b) for G and D modes and Ádány (2004) for L and O modes, and thus apply for all the criterion summarized in Table 1. Since a different **R** matrix may be constructed for each of the modal classes: G, D, L, and O, taken together they span the entire original nodal FSM basis and represent a transformation of the solution from the original nodal basis to a basis where G, D, L, and O deformation fields are segregated, so, for any vector of nodal displacements in global coordinates, **D**:

$$\mathbf{D} = [\mathbf{R_G}\ \mathbf{R_D}\ \mathbf{R_L}\ \mathbf{R_O}]\mathbf{D_r} = \mathbf{R}\mathbf{D_r}$$

represents the transformation. The partitions of the **R** constraint matrices are the deformation fields associated with the G, D, L, and O spaces that meet the

criterion of Table 1, while columns of **R** corresponds to individual deformation modes For the SSMA 600S200-068, **R** for the G, D, and L spaces are provided graphically in Figure 5. For example, the first four deformations in Figure 5a and b provide the warping displacements and transverse displacements for the G modes, i.e.

$$\mathbf{R_G} = [\mathbf{G_1}\ \mathbf{G_2}\ \mathbf{G_3}\ \mathbf{G_4}]$$

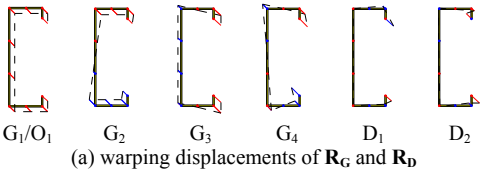

(a) warping displacements of $\mathbf{R_G}$ and $\mathbf{R_D}$

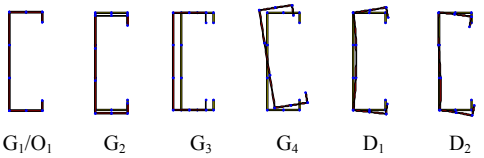

(b) transverse displacements of $\mathbf{R_G}$ and $\mathbf{R_D}$

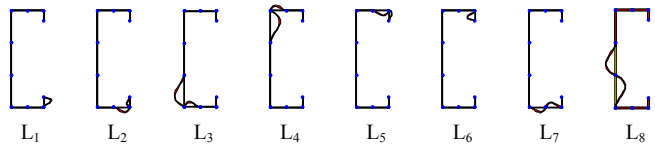

(c) transverse displacements of $\mathbf{R_L}$

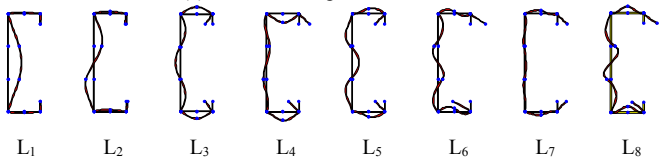

(d) transverse displacements of first 8 $\mathbf{R_{Lu}}$ modes when transformed to unit-member axial modes

Figure 5 Deformation modes spanning G, D, L for SSMA600S200-068 based on *c*FSM

An important characteristic of the $\mathbf{R_G}$ and $\mathbf{R_D}$ deformations is that the transverse displacements are uniquely defined by the warping displacements. For $\mathbf{R_L}$ Figure 5c provides the transverse displacements (note, no warping occurs in the

L modes). As shown, these L modes appear to be in the original FSM nodal DOF basis, but they can be transformed into a modal basis, as discussed below.

Additional transformations inside the G, D, L, O spaces are possible and desirable. One attractive option is to use unit-member axial modes as detailed in Ádány and Schafer (2006b), which, as the name suggests, are the modes for a member of unit-length under axial load within a given space, for example $\mathbf{R_L}$ is transformed to $\mathbf{R_{Lu}}$ as Figure 5d demonstrates. These modes may have physically desirable characteristics in some situations. Finally, the O modes ($\mathbf{R_O}$), associated with shear and transverse extension are not shown here, but are discussed in detail in Ádány (2004) and Schafer and Ádány (2006).

Modal decomposition

In the conventional FSM the complete stability problem is solved. However, in *c*FSM it is possible to constrain the deformations down to only a specific class and thus decompose the modes. For example, consider an analysis focusing only on distortional buckling. Constraint of the deformations from the nodal coordinates to the generalized coordinates in the D space is accomplished by:

$$\mathbf{D} = \mathbf{R_D D_D}$$

Application of this transformation on the eigen stability problem results in a constrained eigen stability problem:

$$\mathbf{R_D}^T\mathbf{K_e R_D}\boldsymbol{\phi}_\mathbf{D} = \lambda\mathbf{R_D}^T\mathbf{K_g R_D}\boldsymbol{\phi}_\mathbf{D} \quad \text{or} \quad \mathbf{K_{eD}}\boldsymbol{\phi}_\mathbf{D} = \lambda\mathbf{K_{gD}}\boldsymbol{\phi}_\mathbf{D}$$

This decomposed stability problem is much smaller than the original stability problem. For the SSMA 600S200-068 example used in this paper the original FSM model consists of 40 DOF, but the decomposed model consists of only 2 DOF – the generalized deformations associated with D_1 and D_2. While the model reduction is potentially beneficial, even better is the reduction in mechanics – restriction to a selected space (e.g., D) allows one to study a mode in detailed ways that cannot be completed in conventional FSM analysis.

The G, D, and L modes are decomposed from the general solution using the procedure described above and the calculated critical forces are plotted against a conventional FSM solution for the 600S200-068 section in Figure 6. The L and mode solution shows excellent agreement with the conventional FSM minima. The D mode solution suggests a somewhat stiffer response than the conventional FSM. For distortional buckling, bending in the web is greater in a conventional FSM than in the decomposed *c*FSM solution (this is shown in the insets to Figure 6, but also may readily be seen in strain energy plots). The relative difference between the conventional FSM minima for D and the *c*FSM solution

is typically smaller in most lipped channels studied by the authors; but in general a difference exists. (Note, this implies a difference between GBT distortional mode solutions and conventional FSM solutions as well). The G mode curve shows the same tendency as a conventional FSM solution, for long members, however the critical loads are somewhat higher. The difference is due to the fact that in-plane transverse deformations are fully restricted in G modes, as discussed in Ádány and Schafer (2006b).

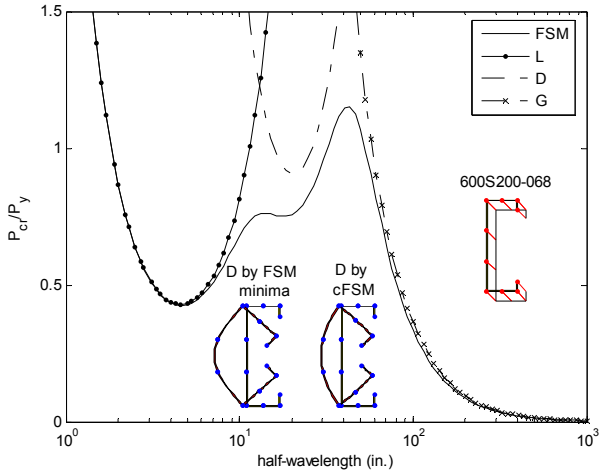

Figure 6 FSM and *c*FSM solutions for SSMA 600S200-068

Modal identification

It is desirable to understand how the different buckling classes (G, D, L, and O) contribute in a conventional FSM stability solution. Indeed, one long-term goal of this research is to provide a classification method that may be used not only in FSM but in general purpose FEM as well. Any displaced shape, **D**, or buckling mode, $\boldsymbol{\phi}$, may be transformed into the basis spanned by the buckling classes through the use of **R**, via

$$\mathbf{D_r} = \mathbf{R}^{-1}\mathbf{D} \quad \text{or} \quad \boldsymbol{\phi}_\mathbf{r} = \mathbf{R}^{-1}\boldsymbol{\phi}$$

where the coefficients in $\mathbf{D_r}$ (or $\boldsymbol{\phi}_\mathbf{r}$) provide the contribution to a given column of **R**, or when summed over columns the contribution in a given class. However, the coefficients are dependent on the normalization of the columns of **R**. A definitive normalization scheme has not been finalized. If $\mathbf{R_i}$ is the i^{th} column vector of **R**, two normalization schemes are considered here.

Vector norm: normalize by setting $||\mathbf{R_i}|| = 1$. Any displacement is expressed as a linear combination: $\boldsymbol{\phi} = \Sigma c_i \mathbf{R_i} = \mathbf{Rc}$, participation, p_i, of mode i is defined by $p_i = |c_i|/\Sigma|c_i|$ where the summation is over all modes.

Weighted strain energy norm: normalize by setting $\frac{1}{2}\mathbf{R_i}^T\mathbf{K_e}\mathbf{R_i} = 1$. Any displacement is expressed as a linear combination: $\boldsymbol{\phi} = \Sigma c_i \mathbf{R_i} = \mathbf{Rc}$, participation, p_i, of mode i is defined by $p_i = |c_i/\lambda_i^{0.5}|/\Sigma|c_i/\lambda_i^{0.5}|$ where the coefficients are weighted by the eigenvalue in that mode alone, i.e. $\lambda_i = \mathbf{R_i}^T\mathbf{K_e}\mathbf{R_i}/\mathbf{R_i}^T\mathbf{K_g}\mathbf{R_i}$.

The contribution of a mode class which spans n columns of **R** is defined as:

$$\sum_{i=1}^{n\ modes} p_i / n$$

Using these definitions (implemented in CUFSM) modal identifications are performed on the SSMAS200-068 and reported in Figure 7. Both methods show the expected regimes of L, D, and G; however it is also clear that the different norms do provide different notions of the response. For instance, at the half-wavelength of the distortional minima L has a non-negligible participation with D. This provides further commentary to the results of Figure 6 where a D only solution for stability proves stiffer than a conventional FSM solution.

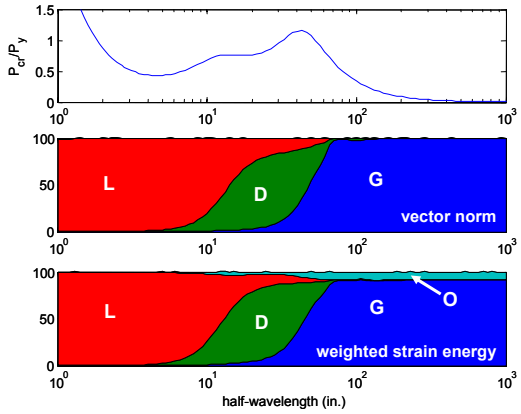

Figure 7 Modal identification results for SSMA 600S200-068

The vector norm is perhaps the simplest possible participation scheme, and it is most similar to that used by GBT; however it lacks a physical basis, is dependent on the discretization of the member, is dependent on the system of units the problem is solved in, and generally discounts the impact of rotations as translations are typically several orders of magnitude larger. The weighted strain

energy norm provides a physically motivated normalization and reasonable identification results. The O mode contribution observed in Figure 7 is consistent with the findings in Schafer and Ádány (2006) which demonstrates that conventional FSM includes an O mode contribution in global buckling.

Discussion

As shown in Figure 6 and Figure 7 minima identified in a conventional FSM solution are not necessarily pure mode solutions. This has ramifications for design methods that employ these critical buckling values. In addition, it further complicates the application of simple qualitative modal identification methods and suggests that quantitative methods such as that provided in *c*FSM are needed. Further discussion of challenges related to *c*FSM is provided in Schafer and Ádány (2006).

Conclusion

The conventional finite strip method combined with the constrained finite strip method provide a powerful tool for exploring cross-section stability in cold-formed steel members. In the conventional finite strip method elastic and geometric stiffness matrices are formed from a summation of cross-section strips and employed in an eigenvalue stability analysis. The stiffness matrices are explicitly derived in this paper and can readily be used in engineering software. The provided solution is identical to that employed in the open source stability analysis program: CUFSM. The constrained finite strip method is described and examples of its application provided. The strength of this new extension to finite strip solutions is the ability to decompose and identify conventional finite strip solutions as related to buckling classes of interest: global, distortional, or local buckling. The examples provided here show the potential use of the constrained finite strip method, and the algorithms discussed are implemented in CUFSM.

Acknowledgments

The presented research has been performed with the financial support of the Korányi Imre Scholarship of the Thomas Cholnoky Foundation, the OTKA K62970 of the Hungarian Scientific Research Fund, the American Iron and Steel Institute, and CMS-0448707 of the United States National Science Foundation.

References

Ádány, S., Schafer, B.W. (2004). "Buckling mode classification of members with open thin-walled cross-sections." Fourth Int'l Conf. on Coupled Instabilities in Metal Structures, Rome, Italy, 27-29 Sept., 2004

Ádány, S., Schafer, B.W. (2006a). "Buckling mode decomposition of single-branched open cross-section members via finite strip method: derivation." Elsevier, *Thin-walled Structures*, (In Press)

Ádány, S., Schafer, B.W. (2006b). "Buckling mode decomposition of single-branched open cross-section members via finite strip method: application and examples." Elsevier, *Thin-walled Structures*, (In Press)

Ádány, S., Slivestre, N., Schafer, B., Camotim, D. (2006). "Buckling analysis of unbranched thin-walled members: generalized beam theory and constrained finite strip method." III European Conference on Computational Mechanics, Solids, Structures and Coupled Problems in Engineering, C.A. Mota Soares et.al. (eds.), Lisbon, Portugal, 5–8 June 2006

Bradford, M.A., Azhari, M. (1995). "Buckling of plates with different end conditions using the finite strip method." *Computers and Structures*, 56 (1) 75-83.

CFS (2006). CFS Version 5.0, RSG Software, www.rsgsoftware.com, visited on April 25, 2006.

Cheung, Y.K., Tham, L.G. (1998). The Finite Strip Method. CRC Press.

NAS (2004). 2004 Supplement to the North American Specification for the Design of Cold-Formed Steel Structures. American Iron and Steel Institute, Washington, DC.

Papangelis, J.P., Hancock, G.J. (1995). "Computer analysis of thin-walled structural members." *Computers & Structures*, Pergamon, 56(1)157-176.

Papangelis, J.P., Hancock, G.J. (2005). Thin-Wall: Cross-Section Analysis and Finite Strip Analysis of Thin-Walled Structures, Thin-Wall v2.1, Centre for Advanced Structural Engineering, University of Sydney, http://www.civil.usyd.edu.au/case/thinwall visited on 15 March 2005.

Rhodes, J. (2002). "Post-buckling analysis of light gauge members using finite strips." Sixteenth International Specialty Conference on Cold-Formed Steel Structures. Orlando, FL USA, October 7-18, 2002.

Schafer, B.W., Ádány, S. (2005). "Understanding and classifying local, distortional and global buckling in open thin-walled members." Tech. Session and Mtg., Structural Stability Research Council. Montreal, Canada.

Schafer, B.W., Ádány, S. (2006). "Modal decomposition for thin-walled member stability using the finite strip method." SMCD 2006, May 14-17, 2006, University of Waterloo, Waterloo, Ontario, Canada

Silvestre, N., Camotim, D. (2002a). "First-order generalised beam theory for arbitrary orthotropic materials." *Thin-Walled Structures*, Elsevier, 40 (9) 755-789.

Silvestre, N., Camotim, D. (2002b). "Second-order generalised beam theory for arbitrary orthotropic materials." *Thin-Walled Structures*, Elsevier, 40 (9) 791-820.